Available online at www.sciencedirect.com
SCIENCE DIRECT®
ELSEVIER
International Journal of Solids and Structures 41 (2004) 6905–6924
INTERNATIONAL JOURNAL OF SOLIDS and STRUCTURES
www.elsevier.com/locate/ijsolstr

Effective elastic properties of solids with two-dimensional inclusions of irregular shapes

Igor Tsukrov *, Jindrich Novak

Department of Mechanical Engineering, University of New Hampshire, Durham, NH 03824, USA

Received 7 December 2003; received in revised form 16 May 2004
Available online 10 July 2004

Abstract

A computational procedure to calculate the contribution of irregularly shaped inclusions into the effective moduli of two-dimensional elastic solids is proposed. This procedure is based on the analysis of a representative volume element subjected to a prescribed macrostress. For each type of inclusion, the compliance contribution tensor is constructed using a combination of Kolosov–Muskhelishvili complex variable technique and numerical conformal mapping. Application of this procedure to regularly shaped inhomogeneities produces results that are in good correspondence with analytical predictions. The effective properties are first derived in the approximation of non-interacting inclusions. Then, several first-order micromechanical models for interacting inclusions are considered.

Keywords: Effective properties; Heterogeneous solids; Rigid inclusions; Elastic inclusions; Conformal mapping

1. Introduction

The ability to determine the effective elastic properties of solids with inhomogeneities is important to predict the overall mechanical behavior of fiber and particle reinforced composites, analyze the interconnect structures of microelectronic circuits, and evaluate the level of damage in parts with microdefects. The approaches to this problem include evaluation of upper and lower bounds (Hashin and Shtrikman, 1962, 1963; Hill, 1963, 1964; Walpole, 1966a,b and later publications), analytical calculations using available elasticity solutions (Eshelby, 1957 and later publications), and direct numerical modeling (for example, finite element analysis) as in Garboczi and Day (1995), Zohdi et al. (1996), Zohdi et al. (2001) and Böhm et al. (2004). Analytical predictions are currently limited to very few regular inclusion shapes (ellipses and polygons in 2D, ellipsoids and polyhedra in 3D). Numerical simulations can be used for practically any geometry and distribution of inclusions. However, they are not convenient when one wants to separate and analyze contributions of different types of inhomogeneities. Also, any modification in positions and relative

* Corresponding author. Tel.: +1-603-862-2086; fax: +1-603-862-1919/1865.
E-mail address: igor.tsukrov@unh.edu (I. Tsukrov).

0020-7683/$ - see front matter © 2004 Elsevier Ltd. All rights reserved.
doi:10.1016/j.ijsolstr.2004.05.037

volumes of inclusions requires new simulations—this can make the parametric studies of microstructures quite consuming.

This paper combines numerical and analytical techniques: the elasticity problem for each type of inclusion is solved numerically, and this solution is used in the analytical procedure of micromechanical modeling. The approach is based on the concept of compliance contribution tensor as described, for example, in Kachanov et al. (1994) and Sevostianov and Kachanov (1999, 2002). The analysis is done in the framework of linear elasticity; inclusions are assumed to be perfectly bonded and randomly distributed in the composite. The effective moduli are first derived in the approximation of non-interacting inclusions. The non-interaction results are then used as a basic building block for several approximate schemes (Mori–Tanaka, self-consistent and differential) in the micromechanical modeling of solids with interacting inclusions.

The effective elastic compliance $\mathbf{S}$ must satisfy the basic relation $\boldsymbol{\varepsilon} = \mathbf{S} : \boldsymbol{\sigma}$ where $\boldsymbol{\varepsilon}$ and $\boldsymbol{\sigma}$ are the second-rank macroscopic strain and stress tensors defined as

$$\boldsymbol{\varepsilon} = \frac{1}{2A}\int_{\gamma} (\mathbf{un} + \mathbf{nu})\,\mathrm{d}\gamma, \qquad \boldsymbol{\sigma} = \frac{1}{A}\int_{\gamma} \mathbf{tx}\,\mathrm{d}\gamma. \tag{1.1}$$

In the equations above, A is the representative area element (RAE) with boundary γ, and $\mathbf{u}$, $\mathbf{n}$, $\mathbf{t}$ and $\mathbf{x}$ are the displacement, outward unit normal, traction and position vectors of the boundary points, respectively, see Fig. 1. Colon denotes contraction over two indices, and $\mathbf{un}$, $\mathbf{nu}$, $\mathbf{tx}$ are the dyadic products of the corresponding vectors.

To characterize the contribution of inclusions to the effective elastic compliance, we introduce the inclusion compliance contribution tensor $\mathbf{H}^{\mathrm{RAE}}$ as

$$\mathbf{S} = \mathbf{S}^{\mathrm{M}} + \mathbf{H}^{\mathrm{RAE}}, \tag{1.2}$$

where $\mathbf{S}^{\mathrm{M}}$ is the compliance tensor of the matrix material. The compliance contribution tensor ($\mathbf{H}$-tensor) was used by Kachanov et al. (1994) and Tsukrov and Novak (2002) to analyze solids with various 2D and 3D holes, and by Sevostianov and Kachanov (1999, 2002) to model solids with elastic ellipsoidal inclusions. The case of elastic polygon-shaped inclusions was considered in Nozaki and Taya (1997, 2001). The effective elastic properties of 2D solids with polygonal and elliptical holes and rigid inclusions were presented in Jasiuk et al. (1994), Jasiuk (1995), Lee (1999) and Tsukrov (2000). Also, extensive literature on elastic properties of solids with circular elastic inclusions (this problem is relevant for composites reinforced by unidirectional fibers of circular cross-section) is available; see for example Hashin and Rosen (1964) and

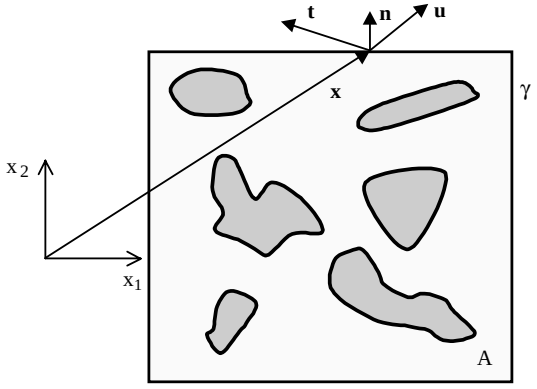

Fig. 1. Representative area element.

Ju and Zhang (1998). Closed form formulae for the ribbon-reinforced composites (modeled as elastic ellipsoidal cylinders) are presented in Zhao and Weng (1990). General considerations and some results on micromechanical modeling of solids with regularly shaped heterogeneities can be found in the books of Mura (1987), Aboudi (1991) and Nemat-Nasser and Hori (1993). In this paper, we present the derivation procedure for **H**-tensors and numerical results for 2D inclusions of *arbitrary irregular shapes*.

The approach is based on the results for one inclusion. We represent the total strain and stress tensors (as defined by Eq. (1.1)) in a reference area $\tilde{A}$ containing an inclusion of area A_I (Fig. 2) as sums

$$\boldsymbol{\varepsilon} = \boldsymbol{\varepsilon}^{M} + \Delta\boldsymbol{\varepsilon}, \qquad \boldsymbol{\sigma} = \boldsymbol{\sigma}^{M} + \Delta\boldsymbol{\sigma}, \tag{1.3}$$

where

$$\boldsymbol{\varepsilon}^{M} = \frac{1}{\tilde{A}} \int_{A_M} \boldsymbol{\varepsilon}(x)\,dA, \qquad \boldsymbol{\sigma}^{M} = \frac{1}{\tilde{A}} \int_{A_M} \boldsymbol{\sigma}(x)\,dA \tag{1.4}$$

are related to the average strain and stress in the matrix as $\boldsymbol{\varepsilon}^{M} = \frac{A_M}{\tilde{A}} \langle \boldsymbol{\varepsilon} \rangle_M$ and $\boldsymbol{\sigma}^{M} = \frac{A_M}{\tilde{A}} \langle \boldsymbol{\sigma} \rangle_M$. Inclusion contributions $\Delta\boldsymbol{\varepsilon}$ and $\Delta\boldsymbol{\sigma}$ are derived from the divergence theorem as:

$$\Delta\boldsymbol{\varepsilon} = -\frac{1}{2\tilde{A}} \int_{\Gamma} (\mathbf{un} + \mathbf{nu})\,d\Gamma, \qquad \Delta\boldsymbol{\sigma} = -\frac{1}{\tilde{A}} \int_{\Gamma} \mathbf{tx}\,d\Gamma, \tag{1.5}$$

where **n** is the unit normal to the inclusion boundary Γ directed inward the inclusion.

Then, the contribution of the inclusion to the overall compliance of $\tilde{A}$ is given by tensor **H**, and the following relation must hold

$$\mathbf{H} : \boldsymbol{\sigma} = \Delta\boldsymbol{\varepsilon} - \mathbf{S}^{M} : \Delta\boldsymbol{\sigma}. \tag{1.6}$$

Tensor **H** possesses the usual symmetries of the elastic compliance tensor ($H_{ijkl} = H_{jilk} = H_{klij}$) and, in 2D case, has no more than six independent components. In the local coordinate system x_1x_2 with unit vectors $\mathbf{e_1}$ and $\mathbf{e_2}$ (Fig. 2), the compliance contribution tensor for an arbitrary 2D inclusion has the following structure

$$\begin{aligned} H = {} & H_{1111}\mathbf{e_1e_1e_1e_1} + H_{2222}\mathbf{e_2e_2e_2e_2} + H_{1122}(\mathbf{e_1e_1e_2e_2} + \mathbf{e_2e_2e_1e_1}) + H_{1211}(\mathbf{e_1e_2e_1e_1} + \mathbf{e_2e_1e_1e_1} \\ & + \mathbf{e_1e_1e_1e_2} + \mathbf{e_1e_1e_2e_1}) + H_{1222}(\mathbf{e_1e_2e_2e_2} + \mathbf{e_2e_1e_2e_2} + \mathbf{e_2e_2e_1e_2} + \mathbf{e_2e_2e_2e_1}) + H_{1212}(\mathbf{e_1e_2e_1e_2} \\ & + \mathbf{e_1e_2e_2e_1} + \mathbf{e_2e_1e_1e_2} + \mathbf{e_2e_1e_2e_1}). \end{aligned} \tag{1.7}$$

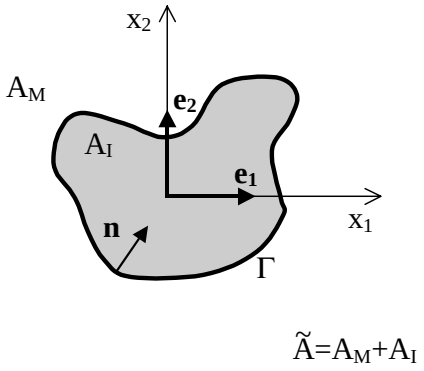

Fig. 2. Inclusion of irregular shape.

To find the components of **H**-tensor for a particular shape, we assume that the total stress in the reference area is equal to the applied remote stress, and evaluate the additional strain and stress tensors. Let us consider a uniaxial tension P inclined at an angle θ to x_1-axis. The stress tensor for such loading is

$$\boldsymbol{\sigma} = P[\cos^2\theta \mathbf{e_1}\mathbf{e_1} + \sin^2\theta \mathbf{e_2}\mathbf{e_2} + \sin\theta\cos\theta(\mathbf{e_1}\mathbf{e_1} + \mathbf{e_2}\mathbf{e_2})]. \tag{1.8}$$

Contraction of this tensor with **H** given by Eq. (1.7) produces the following expressions:

$$\begin{aligned}
(\mathbf{H}:\boldsymbol{\sigma})_{11} &= \frac{P}{2}[(H_{1111}+H_{1122}) + (H_{1111}-H_{1122})\cos 2\theta + 2H_{1211}\sin 2\theta],\\
(\mathbf{H}:\boldsymbol{\sigma})_{22} &= \frac{P}{2}[(H_{2222}+H_{1122}) - (H_{2222}-H_{1122})\cos 2\theta + 2H_{1222}\sin 2\theta],\\
(\mathbf{H}:\boldsymbol{\sigma})_{12} &= \frac{P}{2}[(H_{1211}+H_{1222}) + (H_{1211}-H_{1222})\cos 2\theta + 2H_{1212}\sin 2\theta].
\end{aligned} \tag{1.9}$$

Now, the components of **H** are obtained from Eq. (1.6) by comparing these expressions with the corresponding elasticity predictions for additional strain and stress given by Eq. (1.5) for various values of angle θ.

The constructed **H**-tensors can be utilized to predict the effective elastic moduli using either non-interaction approximation or some first-order micromechanical modeling scheme. In the approximation of non-interacting inclusions, it is assumed that the reference area $\tilde{A}$ of each inclusion is equal to RAE, and the stress field is not disturbed by the presence of other inclusions. Then, the overall response of the material with many non-interacting inclusions can be characterized by the sum of **H**-tensors as

$$\mathbf{S} = \mathbf{S}^{\mathrm{M}} + \mathbf{H}^{\mathrm{NI}}, \tag{1.10}$$

where tensor $\mathbf{H}^{\mathrm{NI}} = \sum \mathbf{H}^{(k)}$ (summation may be replaced by integration over orientations, if computationally convenient) is the non-interaction approximation of tensor $\mathbf{H}^{\mathrm{RAE}}$.

The predictions of more advanced approximate micromechanical schemes can be obtained from $\mathbf{H}^{\mathrm{NI}}$. Detailed discussion on the structure of **H**-tensors in different approximate schemes can be found in Eroshkin and Tsukrov (in press). Section 6 utilizes these results and presents effective moduli of composite materials in several approximations of interacting inclusions.

Thus, the effective elastic properties of composites with irregularly shaped inclusions can be expressed in terms of tensor **H**. To find **H** for each inclusion geometry, the additional strain and stress tensors must be calculated and substituted into Eq. (1.6). This is done by solving the elasticity problem for one inclusion and utilizing Eq. (1.5). In the case of some regular shapes, the elasticity problem can be solved analytically and the explicit expressions for additional strain and stress can be found. Section 2 presents an effective numerical technique to find elasticity solutions for inclusions of highly irregular shapes. The limiting cases of holes and rigid inclusions are covered in Section 3. The non-interaction effective elastic moduli of solids with inclusions of irregular shapes and their mixtures are presented in Sections 4 and 5, correspondingly. Section 6 illustrates how the results of preceding chapters can be utilized to find the effective moduli in the assumption of interacting inclusions.

2. Calculation of the additional strain and stress using numerical conformal mapping

The additional strain and stress due to the presence of an inclusion are found from Eq. (1.5) if the inclusion boundary displacements and tractions under arbitrary loading are known. In 2D elasticity, any stress state can be represented as a sum of two tensions/compressions in principal directions. The numerical technique presented here solves the elasticity problem for a 2D inclusion of arbitrary shape under remotely applied uniform tension. The procedure is based on the complex variable approach (Muskhelishvili, 1963).

It uses the conformal mapping of the exterior of an inclusion onto the interior of a unit circle with the mapping function found by numerical evaluation of the Schwarz–Christoffel integral. Application of this numerical conformal mapping (NCM) method to the analysis of irregularly shaped holes in elastic matrix is described by Tsukrov and Novak (2002).

Note that the analytical solution of the elasticity problem for elliptical inclusion was given by Hardiman (1954). For polygonal shapes, one can use the components of the Eshelby's tensor provided by Rodin (1996), see also Nozaki and Taya (1997, 2001) and Rodin (1998). A complex variable approach to the Eshelby's problem is also presented in Ru (1999). Greengard and Helsing (1998) proposed an efficient numerical algorithm to solve the Sherman integral equation, and applied it to analyze solids with periodic arrangements of irregularly shaped inclusions.

Let us consider an inclusion of arbitrary shape in the complex plane $z = x_1 + \mathrm{i}x_2$ with the origin inside of the inclusion (Fig. 2). The solution requires mapping of the interior of the unit circle in canonical plane ζ onto the exterior of the inclusion region in z plane by analytic mapping function $\omega(\zeta)$. For arbitrary polygons, this can be done by evaluation of the Schwarz–Christoffel integral

$$\omega(\zeta) = \int_{\zeta_1}^{\zeta} \prod_k \left(1 - \frac{\zeta}{\zeta_k}\right)^{1-\beta_k} \frac{1}{\zeta^2}\,\mathrm{d}\zeta, \tag{2.1}$$

where $\beta_k\pi$ are the interior angles of the polygon and ζ_k are the prevertices (points on the unit circle in the canonical plane that correspond to the vertices of the polygon z_k).

We approximate the boundary of the inclusion by N-sided polygon with vertices on the boundary (Fig. 3). The accuracy of this approximation depends on the number of vertices. In the case of regular polygons, the Schwarz–Christoffel integral can be evaluated analytically (Savin, 1961). For more complicated shapes, this integral must be evaluated numerically (we used the Matlab Schwarz–Christoffel toolbox developed by Driscoll (1996)).

The numerical character of the mapping function causes very low accuracy in calculations of the higher order derivatives needed for evaluation of strains and stresses. Therefore, we try to obtain the mapping function in closed form by slight modification in the shape of the approximating polygon. The procedure is described in the next paragraph.

The integrand is expanded in truncated Laurent series with the center at the origin $\zeta = 0$

$$\prod_k \left(1 - \frac{\zeta}{\zeta_k}\right)^{1-\beta_k} \frac{1}{\zeta^2} \cong \sum_{j=-2}^{\mathrm{M}} a_j \zeta^j. \tag{2.2}$$

(Note that the integrand in (2.1) is analytic and single valued in the entire domain of the unit disk except at singular points: prevertexes $\zeta = \zeta_k$ and the origin $\zeta = 0$. Also, coefficient a_{-1} is set to zero to satisfy the single valuedness of the resulting mapping function.) Series (2.2) is convergent in the entire domain of the unit disk except at the specified singular points on the boundary and at the origin. The accuracy of this approximation depends on the number of terms M in the expansion, as illustrated in Fig. 4. As can be seen,

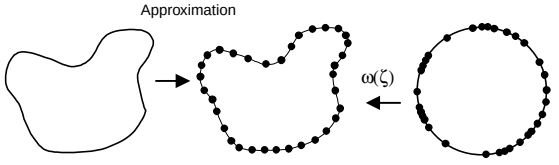

Fig. 3. NCM for the inclusion of irregular shape: points on the boundary correspond to the vertices of the approximating polygon.

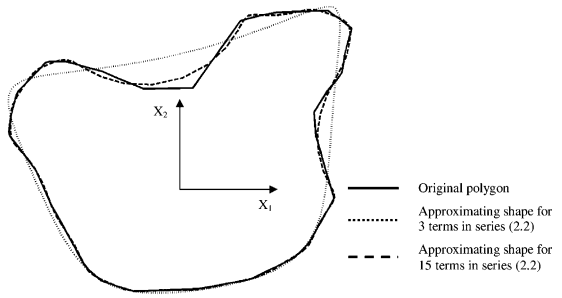

Fig. 4. Approximation of the original shape using mapping function with 3 and 15 terms in series (2.2).

only 15 terms in the expansion are used to achieve relatively good correspondence of the geometries. The mapping function and its derivatives are obtained by integrating and differentiating series (2.2).

Having constructed the mapping function $\omega(\zeta)$, we are able to utilize the Kolosov–Muskhelishvili approach to solve the elasticity problem for a 2D inclusion in an infinite plate loaded by remotely applied uniform tension. According to this approach (Muskhelishvili, 1963), the displacements u, v and stresses σ_{xx}, σ_{yy} and τ_{xy} in the plate and inclusion can be expressed in terms of four analytical functions of complex variable $\varphi_{\mathrm{M}}(\zeta)$, $\psi_{\mathrm{M}}(\zeta)$, $\varphi_{\mathrm{I}}(z)$ and $\psi_{\mathrm{I}}(z)$ (stress functions):

$$
\begin{aligned}
&u^{\mathrm{M}}+\mathrm{i}v^{\mathrm{M}}=\frac{3-\nu_{\mathrm{M}}}{E_{\mathrm{M}}}\varphi_{\mathrm{M}}(\zeta)-\frac{1+\nu_{\mathrm{M}}}{E_{\mathrm{M}}}\left[\frac{\omega(\zeta)}{\overline{\omega'(\zeta)}}\overline{\varphi'_{\mathrm{M}}(\zeta)}+\overline{\psi_{\mathrm{M}}(\zeta)}\right],\\
&\sigma^{\mathrm{M}}_{xx}+\sigma^{\mathrm{M}}_{yy}=4\,\mathrm{Re}\,\frac{\varphi'_{\mathrm{M}}(\zeta)}{\omega'(\zeta)},\\
&\sigma^{\mathrm{M}}_{yy}-\sigma^{\mathrm{M}}_{xx}+2\mathrm{i}\tau^{\mathrm{M}}_{xy}=2\left[\left(\frac{\varphi''_{\mathrm{M}}(\zeta)}{\omega'^{2}(\zeta)}-\varphi'_{\mathrm{M}}(\zeta)\frac{\omega''(\zeta)}{\overline{\omega'^{3}(\zeta)}}\right)\overline{\omega(\zeta)}+\frac{\psi'_{\mathrm{M}}(\zeta)}{\omega'(\zeta)}\right],\\
&u^{\mathrm{I}}+\mathrm{i}v^{\mathrm{I}}=\frac{3-\nu_{\mathrm{I}}}{E_{\mathrm{I}}}\varphi_{\mathrm{I}}(z)-\frac{1+\nu_{\mathrm{I}}}{E_{\mathrm{I}}}\left[z\overline{\varphi'_{\mathrm{I}}(z)}+\overline{\psi_{\mathrm{I}}(z)}\right],\\
&\sigma^{\mathrm{I}}_{xx}+\sigma^{\mathrm{I}}_{yy}=4\,\mathrm{Re}\,\varphi'_{\mathrm{I}}(z),\\
&\sigma^{\mathrm{I}}_{yy}-\sigma^{\mathrm{I}}_{xx}+2\mathrm{i}\tau^{\mathrm{I}}_{xy}=2[\bar{z}\varphi''_{\mathrm{I}}(z)+\psi'_{\mathrm{I}}(z)],
\end{aligned}
\tag{2.3}
$$

where E_{M}, ν_{M} and E_{I}, ν_{I} are the Young's moduli and Poisson's ratios of the matrix and inclusion materials in the case of plane stress. For the plane strain problem, the expressions $E=E/(1-\nu^2)$ and $\nu=\nu/(1-\nu)$ must be substituted instead of E and ν for both matrix and inclusion materials.

The stress functions for the matrix region can be represented in the following form:

$$
\varphi_{\mathrm{M}}(\zeta)=\varphi_{M,1}(\zeta)+\varphi_{M,o}(\zeta),\qquad \psi_{\mathrm{M}}(\zeta)=\psi_{M,1}(\zeta)+\psi_{M,o}(\zeta),
\tag{2.4}
$$

where $\varphi_{M,1}(\zeta)=(P/4)\omega(\zeta)$ and $\psi_{M,1}(\zeta)=-(P/2)\mathrm{e}^{-2\mathrm{i}\theta}\omega(\zeta)$ are the stress functions for the plate without inclusion under uniaxial tension P applied at the infinity at angle θ (Savin, 1961). The additional terms, $\varphi_{M,o}(\zeta)$ and $\psi_{M,o}(\zeta)$, correspond to the disturbance in the stress field caused by the presence of inclusion. We are looking for these additional terms in the form of Taylor series

$$
\varphi_{M,o}(\zeta)=\sum_{n=1}^{\infty}\alpha^{\mathrm{M}}_n\zeta^n,\qquad \psi_{M,o}(\zeta)=\sum_{n=1}^{\infty}\beta^{\mathrm{M}}_n\zeta^n,
\tag{2.5}
$$

that ensure zero rigid body translations and rotation of the infinitely distant parts of the plane and eliminate all indeterminate coefficients from the problem.

The stress functions for the inclusion region, $\varphi_I(z)$ and $\psi_I(z)$, are expanded in series of Faber polynomials $P_n(z)$ that are characteristic for the given domain and must be computed beforehand (we used the Matlab Schwarz–Christoffel toolbox developed by Driscoll (1996)).

$$\varphi_I(z) = \sum_{n=1}^{\infty} \alpha_n^I P_n(z), \qquad \psi_I(z) = \sum_{n=1}^{\infty} \beta_n^I P_n(z). \tag{2.6}$$

Some discussion on the usage of Faber polynomials in the problems of two-dimensional elasticity can be found in Levin and Zingerman (2002).

The coefficients in series (2.5) and (2.6) are calculated from the conditions of continuity of the displacements and boundary force resultants across the interface between the inclusion and matrix:

$$(u + iv)^I = (u + iv)^M, \qquad (f_1 - if_2)^I = (f_1 - if_2)^M. \tag{2.7}$$

Substitution of Eqs. (2.3) and (2.4) into the first equation of (2.7) yields the following form of the displacement continuity condition:

$$\begin{aligned} &-\frac{P(1+\nu_M)}{E_M}\left[\frac{\omega(\zeta)}{4}\left(\frac{3-\nu_M}{1+\nu_M}-1\right)+\frac{e^{2i\theta}}{2}\overline{\omega(\zeta)}\right] \\ &\quad = -\frac{1+\nu_M}{E_M}\left[\frac{\omega(\zeta)}{\overline{\omega'(\zeta)}}\overline{\varphi'_M(\zeta)}+\overline{\psi_M(\zeta)}\right]+\frac{3-\nu_M}{E_M}\varphi_M(\zeta)-\frac{3-\nu_I}{E_I}\varphi_I(z)+\frac{1+\nu_I}{E_I}[z\overline{\varphi'_I(z)}+\overline{\psi_I(z)}]. \end{aligned} \tag{2.8a}$$

Table 1
Components of the compliance contribution tensor **H** for various elastic inclusions $H^*_{ijkl} = (\tilde{A}/A_1)H_{ijkl}$, $E_I = 10^5$ MPa, $E_M = 2 \times 10^4$ MPa and $\nu_I = \nu_M = 0.3$

	H^*_{1111}	H^*_{2222}	H^*_{1212}	H^*_{1122}	H^*_{1211}	H^*_{1222}
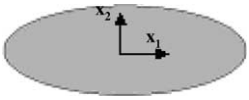	−6.762E−05	−4.805E−05	−3.382E−05	1.768E−05	3.239E−14	−1.352E−13
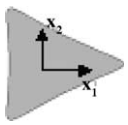	−5.858E−05	−5.855E−06	−3.777E−05	1.698E−05	−1.011E−10	9.874E−10
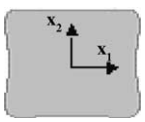	−5.768E−05	−5.769E−05	−3.480E−05	1.788E−05	−7.256E−11	9.095E−11
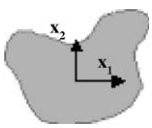	−5.917E−05	−5.443E−05	−3.671E−05	1.627E−05	−1.255E−06	−1.007E−16

The force resultant continuity condition takes the form:

$$-\frac{P}{2}[\omega(\zeta)-e^{2i\theta}\overline{\omega(\zeta)}]=\varphi_{M,o}(\zeta)+\frac{\omega(\zeta)}{\overline{\omega'(\zeta)}}\overline{\varphi'_{M,o}(\zeta)}+\overline{\psi_{M,o}(\zeta)}-\varphi_{I}(z)-z\overline{\varphi'_{I}(z)}-\overline{\psi_{I}(z)}. \tag{2.8b}$$

By requesting that Eqs. (2.8a) and (2.8b) are satisfied at a discrete set of boundary points, we obtain a system of linear equations for unknown coefficients α_n^M, β_n^M, α_n^I, and β_n^I. After this system is solved, the stresses and displacements on the inclusion boundary can be readily obtained from Eq. (2.3). With the above procedure, 60–250 boundary points proved to be sufficient to obtain very accurate results for most of the analyzed shapes.

Knowing the boundary displacements and tractions, we can calculate the components of additional strain and stress tensors for any direction θ of uniaxial tension (by numerically evaluating integrals (1.5)). Repeating this procedure for various angles we find the components of $\Delta\boldsymbol{\varepsilon}$ and $\Delta\boldsymbol{\sigma}$ as numerical functions of θ. The components of **H**-tensor are obtained by comparing these functions with Eq. (1.9). We select a sufficient number of θ values and substitute them into (1.9) together with the corresponding values of $\Delta\boldsymbol{\varepsilon}$ and $\Delta\boldsymbol{\sigma}$. This produces a system of linear equations for components of **H**-tensor. Note that to improve the accuracy, one may choose more values of θ (we used 10) and obtain an overdetermined system of linear equations. The components of **H** are then found by solving this system using the least square method.

Table 1 presents the components of **H**-tensor calculated for selected elastic inclusions with $E_I = 10^5$ MPa and $\nu_I = 0.3$ embedded in the matrix having $E_M = 2 \times 10^4$ MPa and $\nu_M = 0.3$.

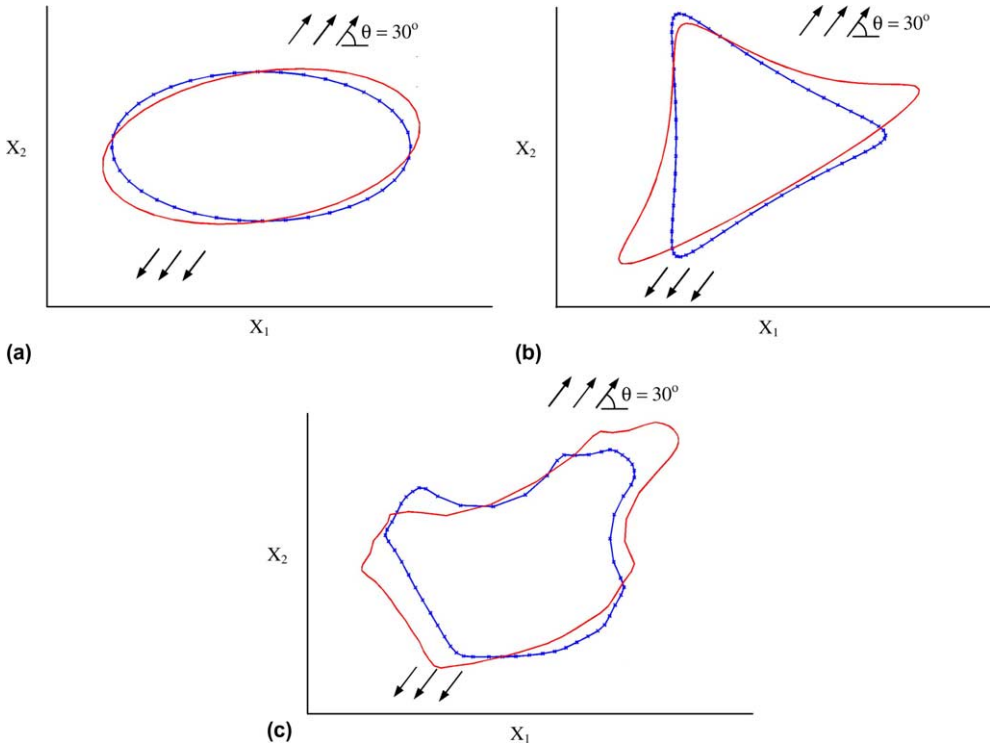

Fig. 5. Deformation of the elastic inclusions under uniaxial tension remotely applied at $\theta = 30°$ with respect to x_1-axis. The boundaries with points represent the undeformed configuration. (a) Ellipse of eccentricity 1:2, (b) 3-cusps hypotrochoid, (c) irregularly shaped inclusion.

Fig. 5 shows these inclusions in both undeformed configuration and under $P = 1$ MPa tension inclined at 30° to x_1 direction. The deformed configuration is given in magnification 60,000:1. The boundaries of the inclusions are discretized using 60 points.

The procedure has been validated by comparing the numerically calculated components of **H**-tensor with the results obtained from available analytical solutions. In the case of elastic elliptical inclusion of eccentricity 2:1 shown in Table 1 (analytical results of Hardiman, 1954), the maximum discrepancy δ evaluated as $(H_{ijkl}^{\mathrm{NCM}} - H_{ijkl}^{\mathrm{Analytical}})/H_{ijkl}^{\mathrm{Analytical}}$ is less than 0.2%. Comparison with available solutions for rigid inclusions and holes is given in Section 3.

3. Inclusion compliance contribution tensor in limiting cases of rigid inclusions and holes

The procedure described in Section 2 can be applied to determine the compliance contribution tensors in the limiting cases of rigid inclusions and holes. Table 2 presents the components of **H**-tensors for rigid inclusions of elliptical (of eccentricity 2:1), triangular-type hypotrochoidal and irregular shape, placed in elastic matrix having $E_{\mathrm{M}} = 5 \times 10^4$ MPa and $\nu_{\mathrm{M}} = 0.3$. Both numerical and analytical results are provided. Analytical expressions for the contribution of regularly shaped rigid inclusions can be obtained based on the results of Hardiman (1954) and Savin (1961).

The effective properties of solids with such inclusions were investigated by Jasiuk (1995) and Tsukrov (2000). Using the **H**-tensor formalism, the contribution of rigid elliptical inclusion with semiaxes a and b is

$$
\begin{aligned}
H_{1111} &= -\frac{\pi}{\tilde{A}E_{\mathrm{M}}}\frac{2a^2 + 3ab + ab\nu_{\mathrm{M}}^2 + 2b^2\nu_{\mathrm{M}}^2}{(3-\nu_{\mathrm{M}})(1+\nu_{\mathrm{M}})},\\
H_{2222} &= -\frac{\pi}{\tilde{A}E_{\mathrm{M}}}\frac{2b^2 + 3ab + ab\nu_{\mathrm{M}}^2 + 2a^2\nu_{\mathrm{M}}^2}{(3-\nu_{\mathrm{M}})(1+\nu_{\mathrm{M}})},\\
H_{1122} &= -\frac{\pi}{\tilde{A}E_{\mathrm{M}}}\frac{ab(1-\nu_{\mathrm{M}}^2) - 2(a+b)^2\nu_{\mathrm{M}}}{(3-\nu_{\mathrm{M}})(1+\nu_{\mathrm{M}})},\\
H_{1212} &= -\frac{\pi}{2\tilde{A}E_{\mathrm{M}}}\frac{ab(a+b)^2(1+\nu_{\mathrm{M}})}{a^2 + ab(1-\nu_{\mathrm{M}}) + b^2}.
\end{aligned}
\tag{3.1}
$$

Table 2
Components of the compliance contribution tensor **H** for various perfectly rigid inclusions $H_{ijkl}^{*} = (\tilde{A}/A_1)H_{ijkl}$, $E_{\mathrm{M}} = 5 \times 10^4$ MPa and $\nu_{\mathrm{M}} = 0.3$

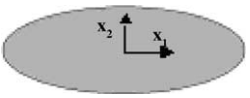

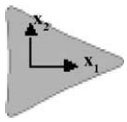

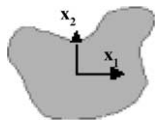

	NCM	Analytical	δ	NCM	Analytical	δ	NCM
H_{1111}^{*}	−4.083E−05	−4.091E−05	−0.002	−3.700E−05	−3.713E−05	−0.003	3.699E−05
H_{2222}^{*}	−2.532E−05	−2.536E−05	−0.001	−3.699E−05	3.713E−05	−0.004	3.176E−05
H_{1212}^{*}	−1.826E−05	−1.828E−05	−0.001	−2.466E−05	−2.476E−05	−0.004	−2.107E−05
H_{1122}^{*}	1.018E−05	1.020E−05	−0.002	1.232E−05	1.240E−05	−0.007	1.117E−05
H_{1211}^{*}	1.994E−14	0	–	−1.508E−09	0	–	−2.009E−06
H_{1222}^{*}	−5.750E−14	0	–	1.492E−09	0	–	−1.055E−07

In the case of triangular-type hypotrochoidal rigid inclusion, the components of **H** are

$$
\begin{aligned}
H_{1111} &= H_{2222} = \frac{A_{\mathrm{I}}}{\tilde{A}E_{\mathrm{M}}}\,\frac{v_{\mathrm{M}}(7-29v_{\mathrm{M}})-(43+7v_{\mathrm{M}})}{7(1+v_{\mathrm{M}})(3-v_{\mathrm{M}})},\\
H_{1122} &= \frac{A_{\mathrm{I}}}{\tilde{A}E_{\mathrm{M}}}\,\frac{v_{\mathrm{M}}(43+7v_{\mathrm{M}})-(7-29v_{\mathrm{M}})}{7(1+v_{\mathrm{M}})(3-v_{\mathrm{M}})},\\
H_{1212} &= \frac{A_{\mathrm{I}}}{\tilde{A}E_{\mathrm{M}}}\,\frac{(7-29v_{\mathrm{M}})-(43+7v_{\mathrm{M}})}{14(3-v_{\mathrm{M}})}.
\end{aligned}
\tag{3.2}
$$

A comparison between our numerical results and analytical predictions given by formulae (3.1) and (3.2) shows good correspondence with the maximum discrepancy δ of 0.7% (Table 2).

Fig. 6 presents rigid inclusions in both original and rotated/translated configuration under remotely applied tension $P = 1$ MPa inclined at 30° with respect to x_1 direction. The displaced configurations are given in magnification 50,000:1. The inclusion boundaries are discretized using the approximating polygon with 60 vertices.

For holes, the geometry and matrix material characteristics in the expressions for the components of **H** decouple (Kachanov et al., 1994). Furthermore, **H**-tensor is independent of the matrix Poisson's ratio. Thus, the material independent *shape factors* $h_1 - h_6$ can be introduced as follows:

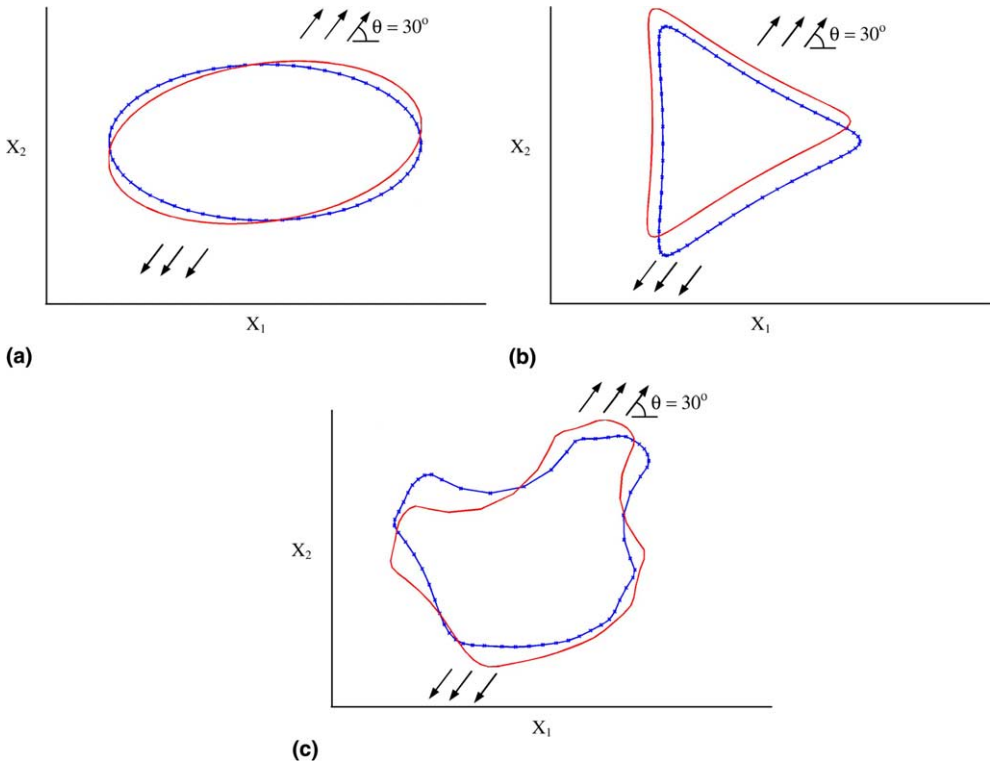

Fig. 6. Rotation (translation) of the rigid inclusions under uniaxial tension remotely applied $\theta = 30°$ with respect to x_1-axis. The boundaries with points represent the original configuration. (a) Ellipse of eccentricity 1:2, (b) triangular-type hypotrochoid, (c) irregularly shaped inclusion.

$$
\begin{aligned}
&h_1 = \frac{E_M\tilde{A}}{A_I}H_{1111}, \quad h_2 = \frac{E_M\tilde{A}}{A_I}H_{2222}, \quad h_4 = \frac{E_M\tilde{A}}{A_I}H_{1122} = \frac{E_M\tilde{A}}{A_I}H_{2211},\\
&h_3 = \frac{2E_M\tilde{A}}{A_I}H_{1212} = \frac{2E_M\tilde{A}}{A_I}H_{1221} = \frac{2E_M\tilde{A}}{A_I}H_{2112} = \frac{2E_M\tilde{A}}{A_I}H_{2121},\\
&h_5 = \frac{E_M\tilde{A}}{A_I}H_{1211} = \frac{E_M\tilde{A}}{A_I}H_{2111} = \frac{E_M\tilde{A}}{A_I}H_{1112} = \frac{E_M\tilde{A}}{A_I}H_{1121},\\
&h_6 = \frac{E_M\tilde{A}}{A_I}H_{1222} = \frac{E_M\tilde{A}}{A_I}H_{2122} = \frac{E_M\tilde{A}}{A_I}H_{2212} = \frac{E_M\tilde{A}}{A_I}H_{2221}.
\end{aligned}
\tag{3.3}
$$

In Tsukrov and Novak (2002), both the NCM procedure and the finite element analysis (FEA) were used to calculate *h*-factors for various regular and irregular hole shapes, and to predict effective properties of porous materials. The NCM results were in good correspondence with the analytical predictions of Kachanov et al. (1994), Jasiuk et al. (1994) and Zimmerman (1991), while FEA estimates were slightly less accurate.

It can be shown by direct substitution that the NCM predictions of the effective elastic properties of solids with cracks and elliptical holes agree with the results reported in Lee et al. (1997) and Lee (1999). This observation also shows a potential of the proposed technique to characterize damage evolution in the case of irregularly shaped defects.

Influence of various inclusion and matrix stiffnesses can also be investigated using the NCM procedure. Fig. 7 presents values of H_{1111} and H_{1212} for triangular-type elastic hyportochoid ($\nu_I = 0.3$) embedded in the elastic matrix having $E_M = 10^4$ MPa and $\nu_M = 0.3$. The Young's modulus of the inclusion varies in the range of $E_I = 10$–10^7 MPa. The *x*-axis of the graph shows inclusion-to-matrix stiffness ratio E_I/E_M on the logarithmic scale. The analytical results of Kachanov et al. (1994) for the hole and Jasiuk (1995) for the rigid inclusion are indicated by stars. Our numerical experiments show that for ratios $E_I/E_M \geqslant 100$ and $E_I/E_M \leqslant 0.01$, the inclusion can be considered as rigid and as a hole, respectively.

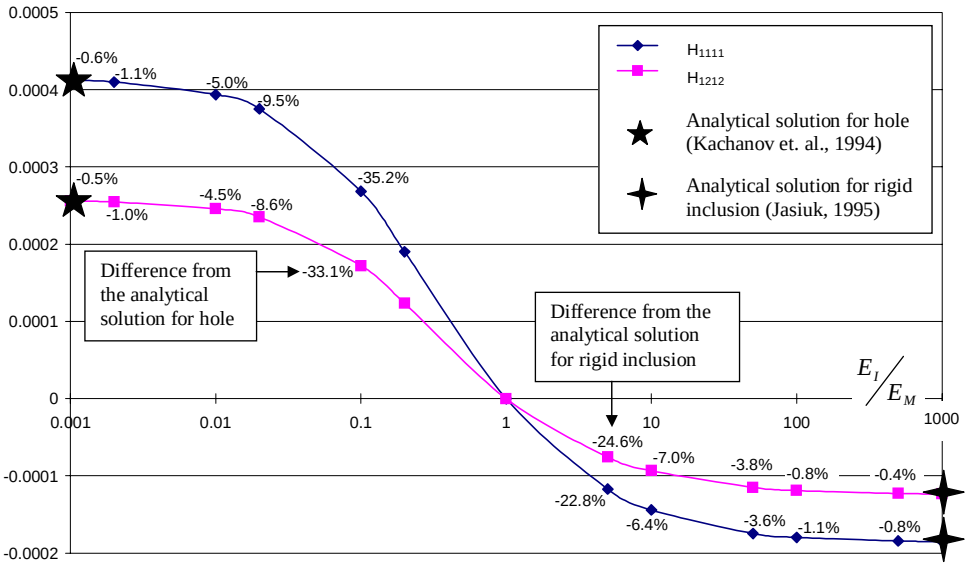

Fig. 7. Variation of **H**-tensor components for triangular-type hypotrochoidal inclusion with the ratio of materials' stiffnesses E_I/E_M ($E_M = 10^4$ MPa and $\nu_I = \nu_M = 0.3$).

4. Effective elastic moduli of solids with many non-interacting inclusions of the same type

This section presents the formulae for the effective elastic properties of 2D solids containing elastic inclusions of identical shape. It is assumed that the location of inclusions is random and uncorrelated with their size and orientation. The predictions are obtained in the non-interaction approximation. This approximation is rigorous at small inclusion densities. As demonstrated in Section 6, it can also be used in some well-developed approximate schemes to predict the effective mechanical properties of solids with interacting inclusions.

In the case of non-symmetrical geometry of an inclusion, **H**-tensor has six independent components as discussed in Section 1. The effective moduli of solids with such inclusions are expressed in terms of the mechanical properties of matrix material, compliance contribution tensor components and inclusion concentration (inclusion volume fraction). The inclusion concentration is defined as

$$f = \frac{1}{A}\sum_k A_{\mathrm{I}}^{(k)}, \tag{4.1}$$

where $A_{\mathrm{I}}^{(k)}$ is the area of the kth inclusion in the representative area A.

Let us apply the procedure described in Section 1 to obtain the effective compliances of the material containing a set of *parallel inclusions* of identical shape. The non-interaction approximation of the overall compliance contribution tensor is equal to the sum of contributions $\mathbf{H}^{(k)}$ from all inclusions. Assuming that the local axes of all inclusions coincide with the global coordinate axes, the contribution of each kth inclusion can be expressed in terms of the same $\mathbf{H}^*$-tensor defined as

$$\mathbf{H}^{(k)} = \frac{A_{\mathrm{I}}^{(k)}}{A}\mathbf{H}^*. \tag{4.2}$$

The components of $\mathbf{H}^*$ for some inclusion shapes are given in Tables 1 and 2.

Utilizing Eq. (1.10), the components of the effective elastic compliance tensor are

$$\begin{aligned} &S_{1111} = \frac{1}{E_{\mathrm{M}}} + fH_{1111}^*, \quad S_{2222} = \frac{1}{E_{\mathrm{M}}} + fH_{2222}^*, \quad S_{1122} = -\frac{\nu_{\mathrm{M}}}{E_{\mathrm{M}}} + fH_{1122}^*, \\ &S_{1212} = \frac{1+\nu_{\mathrm{M}}}{2E_{\mathrm{M}}} + fH_{1212}^*, \quad S_{1211} = fH_{1211}^*, \quad S_{1222} = fH_{1222}^*. \end{aligned} \tag{4.3}$$

Variation of Young's modulus with the orientation of uniaxial tension for a solid with parallel inclusions of irregular shape (as in Fig. 5c) is presented in Fig. 8. The results for circular, triangular and elliptical inclusions ($a/b = 2$) are also shown for comparison. As can be observed, the curve for material with irregular inclusions is not symmetric suggesting that no obvious symmetry of the effective elastic tensor exists. The variation of E/E_{M} for this material is less pronounced than that for the material with elongated (elliptical) inclusions: irregular inclusions (Fig. 5c) introduce less anisotropy into the effective tensor than elliptical of eccentricity 1:2 (Fig. 5a). Thus, deviation from isotropy is dictated by the elongation of the shape rather that the peculiarities of its geometry.

Note that isotropic behavior of composite materials is possible in the case of parallel (or non-randomly oriented) non-interacting inclusions, if the inclusions are *isotropic objects* as discussed in Tsukrov and Novak (2002) and Eroshkin and Tsukrov (in press). The examples of these inclusion shapes include circles and regular polygons with the exception of squares. For such materials, the effective moduli are

$$E = \frac{E_{\mathrm{M}}}{1 + fE_{\mathrm{M}}H_{1111}^*}, \qquad \nu = \frac{\nu_{\mathrm{M}} - E_{\mathrm{M}}fH_{1122}^*}{1 + fE_{\mathrm{M}}H_{1111}^*}. \tag{4.4}$$

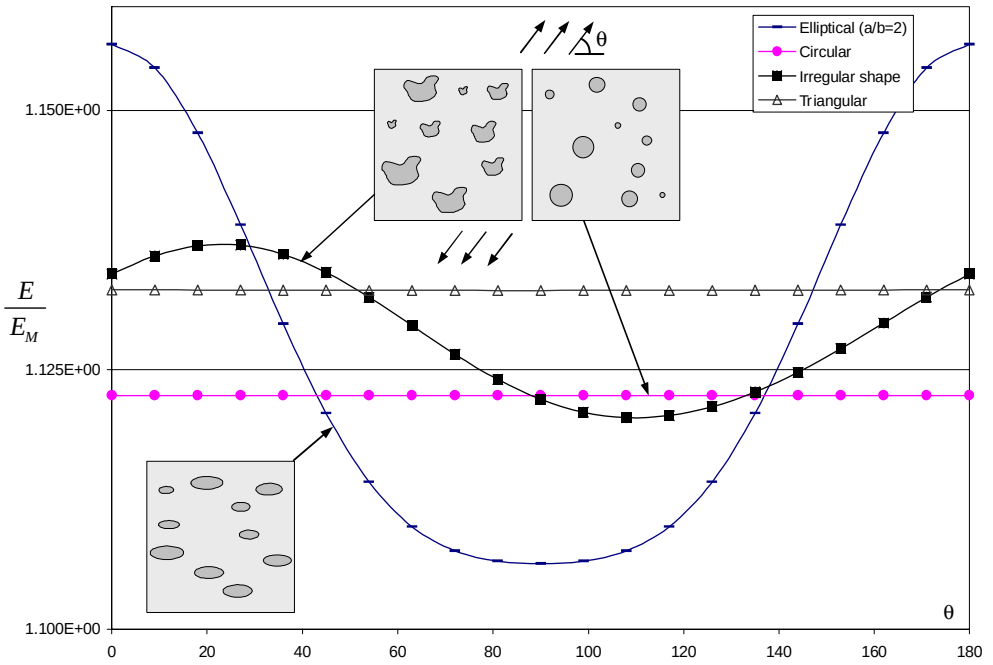

Fig. 8. Variation of the effective Young's modulus with orientation at inclusion concentration $f = 0.1$ ($E_{\mathrm{I}} = 10^5$ MPa, $E_{\mathrm{M}} = 2 \times 10^4$ MPa and $\nu_{\mathrm{I}} = \nu_{\mathrm{M}} = 0.3$).

In Fig. 8, there is no variation of E/E_{M} for circular and triangular inclusion shapes. If inclusions are stiffer than matrix, the circular reinforcement makes composite more compliant than triangular of the same concentration.

When inclusion shapes have two perpendicular axes of geometrical symmetry, the overall properties of material with a set of parallel inclusions are orthotropic. The engineering constants are expressed in terms of the compliance contribution tensor as

$$E_1 = \frac{E_{\mathrm{M}}}{1 + fE_{\mathrm{M}}H^*_{1111}}, \quad E_2 = \frac{E_{\mathrm{M}}}{1 + fE_{\mathrm{M}}H^*_{2222}},$$
$$\nu_{12} = \frac{\nu_{\mathrm{M}} - E_{\mathrm{M}}fH^*_{1122}}{1 + fE_{\mathrm{M}}H^*_{1111}}, \quad G_{12} = \frac{E_{\mathrm{M}}}{2(1 + \nu_{\mathrm{M}} + 2fE_{\mathrm{M}}H^*_{1212})}. \tag{4.5}$$

Materials with *randomly oriented* non-interacting inclusions exhibit isotropic behavior even in the case of highly irregular inclusion shapes. The effective Young's modulus and Poisson's ratio are (note that only four out of six independent components of **H** are present):

$$E = \frac{E_{\mathrm{M}}}{1 + fE_{\mathrm{M}}\left[\frac{3}{8}(H^*_{1111} + H^*_{2222}) + \frac{1}{4}(2H^*_{1212} + H^*_{1122})\right]},$$
$$\nu = \frac{\nu_{\mathrm{M}} - fE_{\mathrm{M}}\left[\frac{1}{8}(H^*_{1111} + H^*_{2222}) + \frac{3}{4}H^*_{1122} - \frac{1}{2}H^*_{1212}\right]}{1 + fE_{\mathrm{M}}\left[\frac{3}{8}(H^*_{1111} + H^*_{2222}) + \frac{1}{4}(2H^*_{1212} + H^*_{1122})\right]}. \tag{4.6}$$

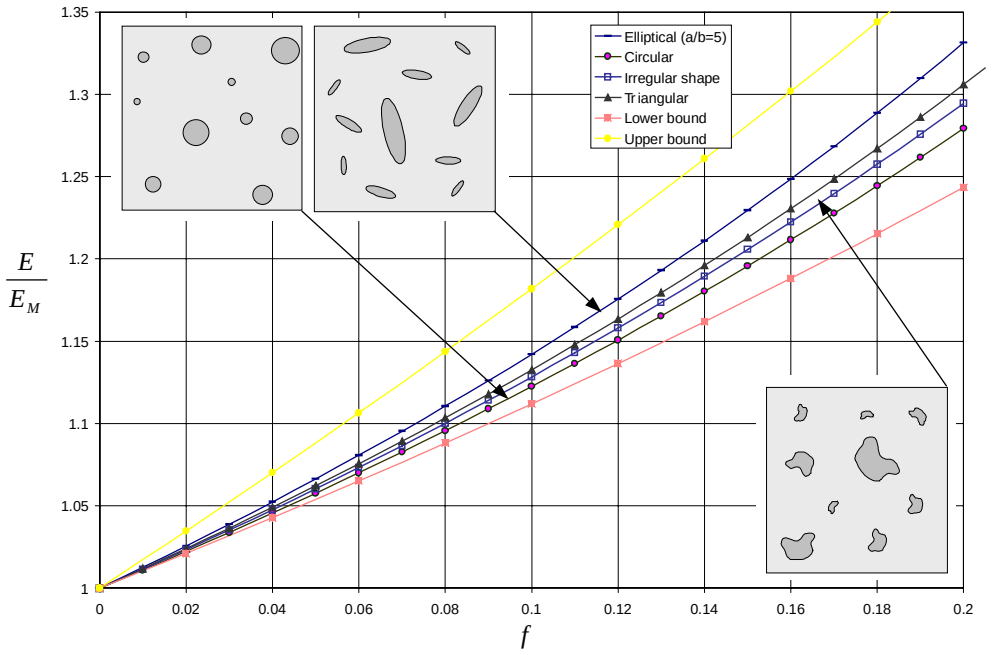

Fig. 9. Effective Young's modulus as function of inclusion concentration for material with randomly oriented elastic inclusions ($E_I = 10^5$ MPa, $E_M = 2 \times 10^4$ MPa and $\nu_I = \nu_M = 0.3$).

For example, the effective Young's modulus of the elastic solid containing randomly oriented irregular inclusions of the shape shown in Fig. 5c can be obtained using the values of **H**-tensor components presented in Table 1. Fig. 9 illustrates the dependence of E/E_M on the inclusion concentration for $E_I = 10^5$ MPa, $E_M = 2 \times 10^4$ MPa and $\nu_I = \nu_M = 0.3$. Comparison with circular and elongated elliptical shapes ($a/b = 5$) shows that for randomly oriented and randomly located non-interacting inclusions that are stiffer than matrix, the more elongated shapes produce higher increase in the effective stiffness. Note that all the curves in Fig. 9 lie within the bounds provided by Hill (1964).

5. Effective elastic moduli of solids with a mixture of non-interacting inclusions of various types

In this section, we consider materials with a mixture of inclusions of different shapes. The effective moduli of such materials are presented in terms of *partial inclusion concentrations*

$$f_N = \frac{1}{A} \sum_k A_{I,N}^{(k)}, \tag{5.1}$$

where $A_{I,N}^{(k)}$ refers to the area of inclusion having geometry of Nth type. If a material contains several sets of parallel inclusions with the inclusions of Nth type inclined at angle θ_N with respect to x_1 axis of the global coordinate system x_1x_2, the effective compliances are as follows:

$$
\begin{aligned}
S_{1111} &= \frac{1}{E_{\mathrm{M}}} + \sum_N f_N [m^4 H^*_{1111} + n^4 H^*_{2222} + 2m^2 n^2 (H^*_{1122} + 2H^*_{1212}) - 4m^3 n H^*_{1211} - 4mn^3 H^*_{1222}]_N,\\
S_{2222} &= \frac{1}{E_{\mathrm{M}}} + \sum_N f_N [n^4 H^*_{1111} + m^4 H^*_{2222} + 2m^2 n^2 (H^*_{1122} + 2H^*_{1212}) + 4mn^3 H^*_{1211} + 4m^3 n H^*_{1222}]_N,\\
S_{1122} &= -\frac{\nu_{\mathrm{M}}}{E_{\mathrm{M}}} + \sum_N f_N [m^2 n^2 (H^*_{1111} + H^*_{2222}) + (m^4 + n^4) H^*_{1122} - 4m^2 n^2 H^*_{1212} + 2(m^3 n - mn^3) H^*_{1211}\\
&\quad + 2(mn^3 - m^3 n) H^*_{1222}]_N,\\
S_{1212} &= \frac{1 + \nu_{\mathrm{M}}}{2E_{\mathrm{M}}} + \sum_N f_N [m^2 n^2 (H^*_{1111} + H^*_{2222}) - 2m^2 n^2 H^*_{1122} + (m^4 - 2m^2 n^2 + n^4) H^*_{1212}\\
&\quad + 2(m^3 n - mn^3) H^*_{1211} + 2(mn^3 - m^3 n) H^*_{1222}]_N,\\
S_{1211} &= \sum_N f_N [m^3 n (H^*_{1111} - H^*_{1122} - 2H^*_{1212}) + mn^3 (-H^*_{2222} + H_{1122} + 2H^*_{1212}) + (m^4 - 3m^2 n^2) H^*_{1211}\\
&\quad + (-n^4 - 3m^2 n^2) H^*_{1222}]_N,\\
S_{1222} &= \sum_N f_N [m^3 n (-H^*_{2222} + H^*_{1122} + 2H^*_{1212}) + mn^3 (H^*_{1111} - H^*_{1122} - 2H^*_{1212}) + (-n^4 + 3m^2 n^2) H^*_{1211}\\
&\quad + (m^4 - 3m^2 n^2) H^*_{1222}]_N,
\end{aligned}
\tag{5.2}
$$

where $(H^*_{1111}, H^*_{2222}, \ldots)_N$ are the components of the compliance contribution tensor of the inclusions of Nth type, $m_N = \cos\theta_N$ and $n_N = \sin\theta_N$.

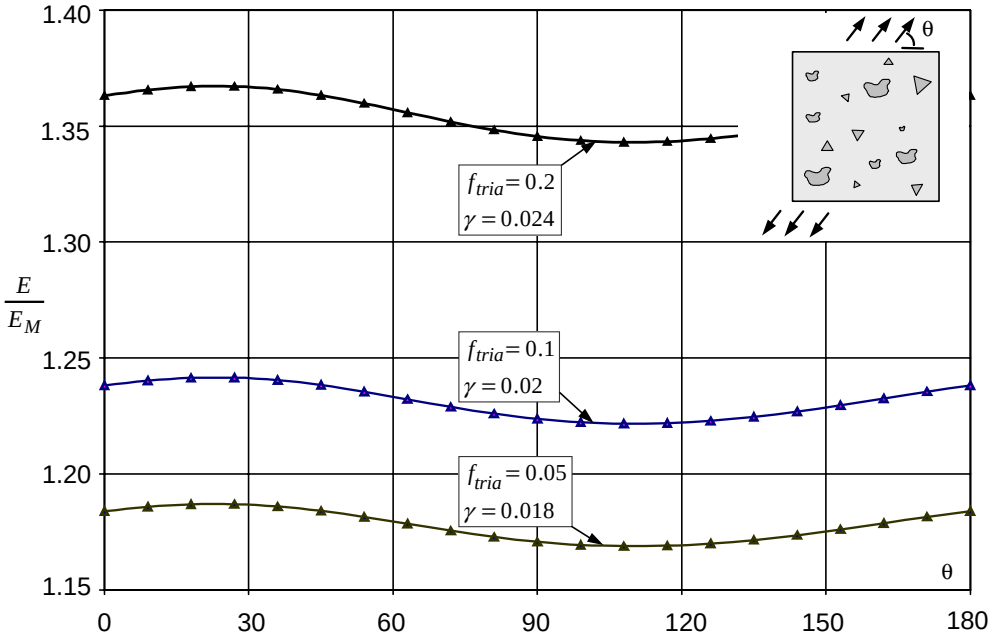

Fig. 10. Variation of Young's modulus with orientation for material with mixture of rigid triangular inclusions and parallel elastic inclusions of irregular shape ($f_{\mathrm{irreg}} = 0.1$, $E_{\mathrm{I}} = 10^5$ MPa, $E_{\mathrm{M}} = 2 \times 10^4$ MPa and $\nu_{\mathrm{I}} = \nu_{\mathrm{M}} = 0.3$).

The effective elastic properties of the material with a mixture of randomly oriented inclusions are isotropic. The effective Young's modulus and Poisson's ratio are

$$E = \frac{E_{\mathrm{M}}}{1 + E_{\mathrm{M}} \sum\limits_{N} f_N \left(\frac{3}{8}(H^*_{1111} + H^*_{2222}) + \frac{1}{4}(2H^*_{1212} + H^*_{1122}) \right)_N},$$
$$\nu = \frac{\nu_{\mathrm{M}} - E_{\mathrm{M}} \sum\limits_{N} f_N \left(\frac{1}{8}(H^*_{1111} + H^*_{2222}) + \frac{3}{4}(H^*_{1122} - \frac{1}{2}H^*_{1212}) \right)_N}{1 + E_{\mathrm{M}} \sum\limits_{N} f_N \left(\frac{3}{8}(H^*_{1111} + H^*_{2222}) + \frac{1}{4}(2H^*_{1212} + H^*_{1122}) \right)_N}. \tag{5.3}$$

As an example, we consider the variation of Young's modulus with orientation for the material with a mixture of randomly oriented rigid triangular inclusions and parallel elastic irregular inclusions (of type shown in Fig. 5c) for $E_{\mathrm{I}} = 10^5$ MPa, $E_{\mathrm{M}} = 2 \times 10^4$ MPa and $\nu_{\mathrm{I}} = \nu_{\mathrm{M}} = 0.3$. The concentration of irregular inclusions is fixed at $f_{\mathrm{irreg}} = 0.1$, and the concentration of triangular inclusions, f_{tria}, varies from 0.05 to 0.2. Note that triangular inclusions are *isotropic* objects as mentioned in Section 4, so neither parallel nor randomly oriented inclusions of this type alone introduce any anisotropy. But, as can be seen from Fig. 10, the increase in the concentration of triangular inclusions in the presence of parallel inclusions raises the overall anisotropy: parameter $\gamma = (E_{\max} - E_{\min})/E_{\mathrm{M}}$ changes from 0.018 for $f_{\mathrm{tria}} = 0.05$ to 0.024 for $f_{\mathrm{tria}} = 0.2$.

6. Micromechanical modeling of solids with interacting inclusions

The results of the preceding sections are obtained in the approximation of non-interacting inclusions. They can be used to predict the effective elastic properties when interaction between the inclusions is

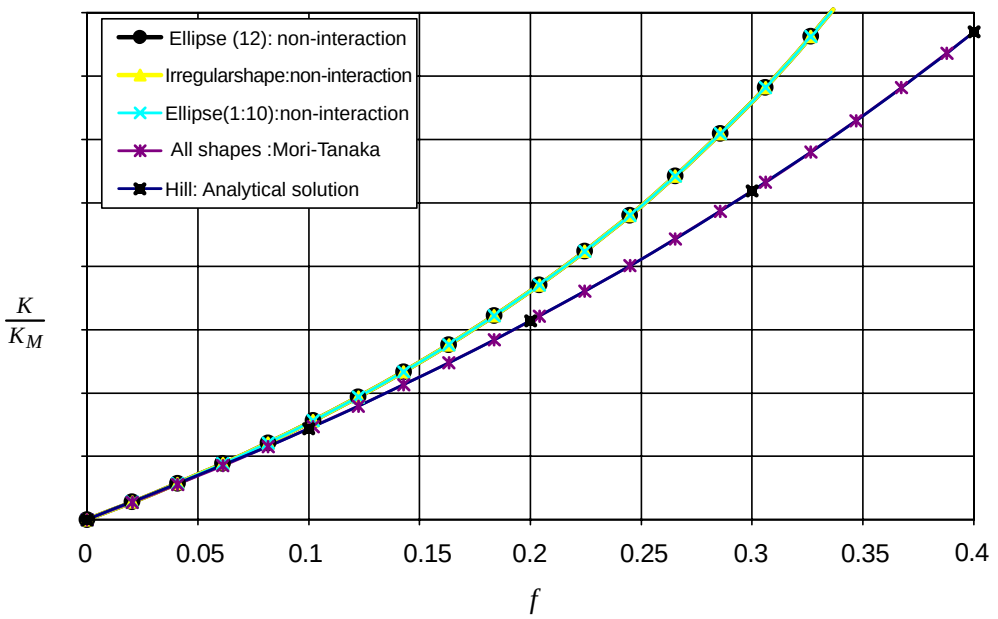

Fig. 11. Effective bulk modulus of composite material with phases of identical shear moduli ($E_{\mathrm{I}} = 63.043$ GPa, $\nu_{\mathrm{I}} = 0.45$, $E_{\mathrm{M}} = 50$ GPa and $\nu_{\mathrm{M}} = 0.15$). Inclusions are stiffer than matrix.

approximated by any of the well-developed first order micromechanical schemes (self-consistent, Mori–Tanaka, etc.). Let us consider a two-phase composite with arbitrarily shaped inclusions of compliance $\mathbf{S}^{\mathrm{I}}$ homogeneously dispersed in the matrix material. It is assumed that location of the inclusions is uncorrelated with their size and orientations. The micromechanical predictions can then be obtained from $\mathbf{H}^{\mathrm{NI}}$ (Eroshkin and Tsukrov, in press). In the case of Mori–Tanaka approximation, when each inclusion is assumed to be subjected to the remote stress equal to the average stress in the matrix phase, the compliance contribution tensor $\mathbf{H}^{\mathrm{MT}}$ and the effective compliance $\mathbf{S}$ are

$$\mathbf{H}^{\mathrm{MT}} = \mathbf{H}^{\mathrm{NI}} : [(1-f)(\mathbf{S}^{\mathrm{I}} - \mathbf{S}^{\mathrm{M}}) + \mathbf{H}^{\mathrm{NI}}]^{-1} : (\mathbf{S}^{\mathrm{I}} - \mathbf{S}^{\mathrm{M}}), \quad \mathbf{S} = \mathbf{S}^{\mathrm{M}} + \mathbf{H}^{\mathrm{MT}}. \tag{6.1}$$

Self-consistent method assumes the inclusions to be placed in the equivalent matrix having the overall property of composite $\mathbf{S}$:

$$\mathbf{H}^{\mathrm{SC}} = (\mathbf{S}^{\mathrm{I}} - \mathbf{S}^{\mathrm{M}}) : (\mathbf{S}^{\mathrm{I}} - \mathbf{S})^{-1} : \mathbf{H}^{\mathrm{NI}}(\mathbf{S}, \mathbf{S}^{\mathrm{I}}), \quad \mathbf{S} = \mathbf{S}^{\mathrm{M}} + \mathbf{H}^{\mathrm{SC}}. \tag{6.2}$$

where $\mathbf{H}^{\mathrm{NI}}(\mathbf{S}, \mathbf{S}^{\mathrm{I}})$ is the non-interaction compliance contribution tensor when inclusion $\mathbf{S}^{\mathrm{I}}$ is placed into matrix $\mathbf{S}$. In the differential method, the non-interacting inclusions are incrementally added to the material until the final inclusion volume fraction f is reached. The $\mathbf{H}$-tensor and effective compliance are found from differential equation

$$\frac{\mathrm{d}\mathbf{H}^{\mathrm{DIFF}}}{\mathrm{d}t} = \frac{1}{f(1-t)} \mathbf{H}^{\mathrm{NI}}(\mathbf{S}(t), \mathbf{S}^{\mathrm{I}}), \quad \mathbf{S} = \mathbf{S}^{\mathrm{M}} + \mathbf{H}^{\mathrm{DIFF}}, \tag{6.3}$$

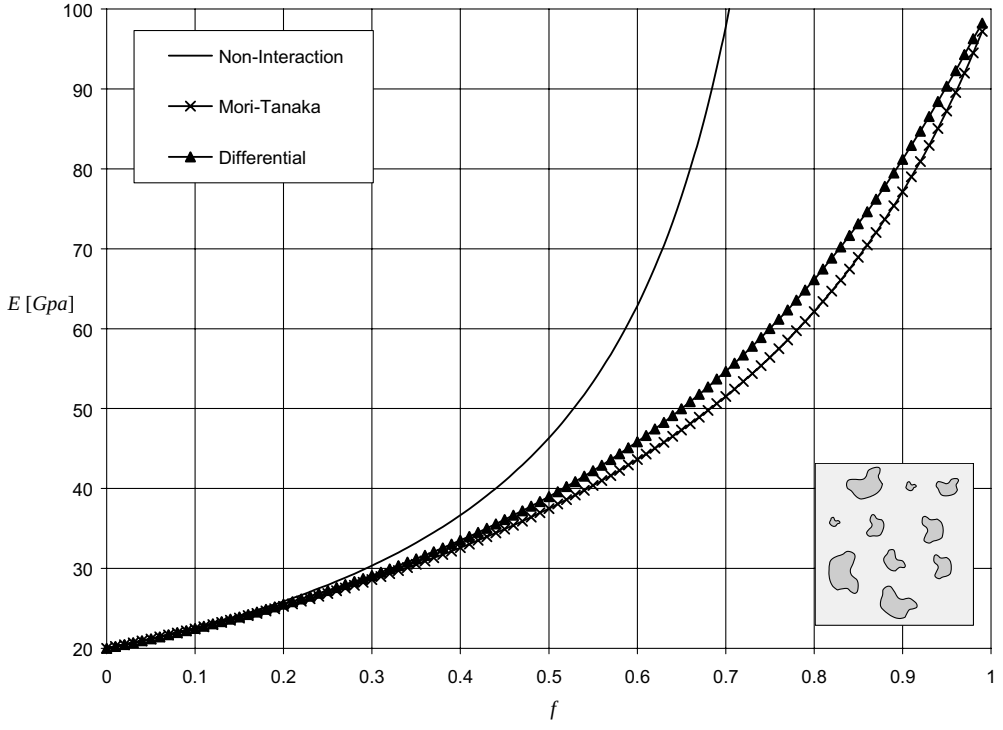

Fig. 12. Predictions of the effective Young's modulus by various approximate schemes ($E_{\mathrm{I}} = 100$ GPa, $E_{\mathrm{M}} = 20$ GPa and $\nu_{\mathrm{I}} = \nu_{\mathrm{M}} = 0.3$).

where $\mathbf{S}(t)$ denotes the compliance of the composite having inclusion volume fraction t. Eq. (6.3) is solved with the initial condition $\mathbf{H}^{\mathrm{DIFF}}(t=0)=0$.

Fig. 11 shows the Mori–Tanaka and non-interaction estimates of the effective bulk modulus of the unidirectional composite (plane strain) with two phases having identical shear moduli $G=21.739$ GPa ($v_{\mathrm{I}}=0.45$ and $v_{\mathrm{M}}=0.15$). In this case, the components of $\mathbf{H}$-tensor are the same for all inclusion shapes, and the Mori–Tanaka prediction coincides with the analytical solution of Hill (1964), which is given by the following formula:

$$K=\frac{f_{\mathrm{I}}K_{\mathrm{I}}(K_{\mathrm{M}}+G)+(1-f_{\mathrm{I}})K_{\mathrm{M}}(K_{\mathrm{I}}+G)}{f_{\mathrm{I}}(K_{\mathrm{M}}+G)+(1-f_{\mathrm{I}})(K_{\mathrm{I}}+G)}. \tag{6.4}$$

Fig. 12 illustrates application of the differential and Mori–Tanaka approximate schemes to a 2D solid with interacting inclusions of irregular shape shown in Fig. 5c ($E_{\mathrm{I}}=100$ GPa and $v_{\mathrm{I}}=0.3$) inserted in a matrix material ($E_{\mathrm{M}}=20$ GPa and $v_{\mathrm{M}}=0.3$). As can be seen, the Mori–Tanaka approach predicts the most compliant response of the composite material. This result is in agreement with the observation of Dvorak and Srinivas (1999) that Mori–Tanaka estimates constitute a lower bound when inclusions are stiffer than matrix.

7. Conclusions

Contribution of the irregularly shaped inclusions to the effective elastic moduli of two-dimensional composites can be evaluated using the numerical conformal mapping procedure. First, the inclusion compliance contribution tensor is found for the individual inclusion of a given shape. This is done by substitution of the numerically calculated components of the additional strain and stress tensors in Eq. (1.6). In the assumption of non-interacting inclusions, the overall compliance contribution tensor $\mathbf{H}^{\mathrm{NI}}$ is obtained by direct summation of contributions of all inclusions in the representative area. When mixtures of inclusions of different types are present in the material, this tensor is expressed in terms of partial inclusion concentrations. $\mathbf{H}^{\mathrm{NI}}$ tensor can also be used in the first order micromechanical models to predict the effective elastic properties of materials with interacting inclusions.

The NCM procedure to solve the elasticity problem for an inclusion is based on the Kolosov–Muskhelishvili complex variable approach. It requires numerical construction of the conformal mapping function in the form of Schwarz–Christoffel integral. The computationally effective and stable algorithm involves the approximation of the integrand by a truncated Laurent series. The complex potentials (stress functions) are expanded in Taylor series in the matrix region, and in the series of Faber polynomials in the inclusion domain. The unknown coefficients in the expansions are then obtained by satisfying the stress and displacement continuity conditions across the interface of the inclusion and matrix regions.

Application of the procedure to the limiting cases of holes and perfectly rigid inclusions produces results that are in good agreement with known analytical solutions. The maximum observed discrepancy for the rigid inclusions approximated by 60 boundary points is less than 1%. Comparison with the results based on Hardiman's solution for elastic elliptical inclusion yields even better accuracy of 0.2%. Also, our numerical simulations show that for the ratios $E_{\mathrm{I}}/E_{\mathrm{M}}\geqslant 100$ and $E_{\mathrm{I}}/E_{\mathrm{M}}\leqslant 0.01$, the inclusion can be considered as rigid and as a hole, respectively.

Non-random orientation of the irregularly shaped inclusions results in anisotropy of the overall properties. It is observed, that for this anisotropy, the peculiarities of the inclusion shapes are not as important as their elongation in general. Also, for the inclusions that are stiffer than matrix, the same concentration of more elongated shapes produces a stiffer composite. For the inclusions that are softer than matrix, the effect is opposite.

Acknowledgements

This research was partially supported by the DMII Division of the National Science Foundation through the grant #0300216 to the University of New Hampshire. The authors would also like to acknowledge O. Eroshkin's participation in the calculations presented in Section 6.

References

Aboudi, J., 1991. Mechanics of Composite Materials. Elsevier.

Böhm, H.J., Han, W., Eckschlager, A., 2004. Multi-inclusion unit cell studies of reinforcement stresses and particle failure in discontinuously reinforced ductile matrix composites. CMES—Computer Modeling in Engineering and Science 5, 5–20.

Driscoll, T.A., 1996. A MATLAB Toolbox for Schwarz–Christoffel mapping. ACM Transactions on Mathematical Software 22, 168–186.

Dvorak, G.J., Srinivas, M.V., 1999. New estimates of overall properties of heterogeneous solids. Journal of the Mechanics and Physics of Solids 47, 899–920.

Eroshkin, O., Tsukrov, I., in press. On micromechanical modeling of three-dimensional solids with irregularly shaped inclusions. International Journal of Solids and Structures.

Eshelby, J.D., 1957. The determination of the elastic field of an ellipsoidal inclusion, and related problems. In: Proceedings of The Royal Society of London Series A, 241, pp. 376–396.

Garboczi, E.J., Day, A.R., 1995. An algorithm for computing the effective linear elastic properties of heterogeneous materials: three-dimensional results for composites with equal phase Poisson ratios. Journal of the Mechanics and Physics of Solids 43 (9), 1349–1362.

Greengard, L., Helsing, J., 1998. On the numerical evaluation of elastostatic fields in locally isotropic two-dimensional composites. Journal of the Mechanics and Physics of Solids 46 (8), 1441–1462.

Hardiman, N.J., 1954. Elliptic elastic inclusion in an infinite elastic plate. Quarterly Journal of Mechanics and Applied Mathematics 7 (2), 226–230.

Hashin, Z., Rosen, B.W., 1964. The elastic moduli of fiber-reinforced materials. Journal of Applied Mechanics 31, 223–232.

Hashin, Z., Shtrikman, S., 1963. A variational approach to the theory of the elastic behavior of multiphase materials. Journal of the Mechanics and Physics of Solids 11, 127–140.

Hashin, Z., Shtrikman, S., 1962. On some variational principles in anisotropic and non-homogeneous elasticity. Journal of the Mechanics and Physics of Solids 10, 335–342.

Hill, R., 1963. Elastic properties of reinforced solids: some theoretical approaches. Journal of the Mechanics and Physics of Solids 11, 357–372.

Hill, R., 1964. Theory of mechanical properties of fibre-strengthened materials: I. Elastic behavior. Journal of the Mechanics and Physics of Solids 12, 199–212.

Jasiuk, I., 1995. Cavities vis-à-vis rigid inclusions: Elastic moduli of materials with polygonal inclusions. International Journal of Solids and Structures 32 (3/4), 407–422.

Jasiuk, I., Chen, J., Thorpe, M.F., 1994. Elastic moduli of two dimensional materials with polygonal elliptical holes. Applied Mechanics Reviews 47 (1), 18–28.

Ju, J.W., Zhang, X.D., 1998. Micromechanics and effective transverse elastic moduli of composites with randomly located aligned circular fibers. International Journal of Solids and Structures 35 (9–10), 941–960.

Kachanov, M., Tsukrov, I., Shafiro, B., 1994. Effective properties of solids with cavities of various shapes. Applied Mechanics Reviews 47 (1), 151–174.

Lee, U., 1999. Effective elastic compliances and engineering constants for damaged isotropic solids. International Journal of Damage Mechanics 8, 138–152.

Lee, U., Lesieutre, G.A., Fang, L., 1997. Anisotropic damage mechanics based on strain energy equivalence and equivalent elliptical microcracks. International Journal of Solids and Structures 34, 4377–4397.

Levin, V.A., Zingerman, V.M., 2002. Plane problems of the theory of repeated superposition of large deformations. Fizmatlit, Moscow, Russia.

Muskhelishvili, N.I., 1963. Some Basic Problems of Mathematical Theory of Elasticity. Noordhoff, Groningen.

Mura, T., 1987. Micromechanics of Defects in Solids. Kluwer, Dodrecht, The Netherlands.

Nemat-Nasser, S., Hori, M., 1993. Micromechanics: Overall Properties of Heterogeneous Materials. North-Holland.

Nozaki, H., Taya, M., 1997. Elastic fields in a polygon-shaped inclusion with uniform eigenstrains. Journal of Applied Mechanics 64, 495–502.

Nozaki, H., Taya, M., 2001. Elastic fields in a polyhedral inclusion with uniform eigenstrains and related problems. Journal of Applied Mechanics 68, 441–452.

Rodin, G.J., 1996. Eshelby's inclusion problem for polygons and polyhedra. Journal of the Mechanics and Physics of Solids 44 (12), 1977–1995.

Rodin, G.J., 1998. Elastic fields in a polygon shaped inclusions with uniform eigenstrains. Translations of the ASME, Journal of Applied Mechanics 65, 278.

Ru, C.Q., 1999. Analytic solution for Eshelby's problem of an inclusion of arbitrary shape in a plane or half-plane. Journal of Applied Mechanics 66, 315–322.

Savin, G.N., 1961. Stress concentration around holes, Volume 1, International Series of Monographs on Aeronautics and Astronautics. Pergamon Press, London.

Sevostianov, I., Kachanov, M., 1999. Compliance tensors of ellipsoidal inclusions. International Journal of Fracture 96, L3–L7.

Sevostianov, I., Kachanov, M., 2002. Explicit cross-property correlations for anisotropic two-phase composite materials. Journal of the Mechanics and Physics of Solids 50, 253–282.

Tsukrov, I., 2000. Elastic moduli of composites with rigid elliptical inclusions. International Journal of Fracture 101, L29–L34.

Tsukrov, I., Novak, J., 2002. Effective elastic properties of solids with defects of irregular shapes. International Journal of Solids and Structures 39, 1539–1555.

Walpole, L.J., 1966a. On bounds for the overall elastic moduli of inhomogeneous systems—I. Journal of the Mechanics and Physics of Solids 14, 151–162.

Walpole, L.J., 1966b. On bounds for the overall elastic moduli of inhomogeneous systems—II. Journal of the Mechanics and Physics of Solids 14, 289–301.

Zhao, Y.H., Weng, G.J., 1990. Effective elastic moduli of ribbon-reinforced composites. Journal of Applied Mechanics 57, 158–167.

Zimmerman, R.W., 1991. Compressibility of Sandstones. Elsevier, Amsterdam.

Zohdi, T.I., Oden, J.T., Rodin, G.J., 1996. Hierarchical modeling of heterogeneous bodies. Computer Methods in Applied Mechanics and Engineering 138, 273–298.

Zohdi, T.I., Wriggers, P., Huet, C., 2001. A method of substructuring large-scale computational micromechanical problems. Computer Methods in Applied Mechanics and Engineering 190, 5639–5656.